Si $2p$ photoabsorption in SiH_4 and SiD_4: Molecular distortion in core-excited silane

R. Püttner,[1] M. Domke,[1] D. Lentz,[2] and G. Kaindl[1]
[1]*Institute for Experimental Physics and Material Science Center, Freie Universität Berlin, Arnimalllee 14, D-14195 Berlin-Dahlem, Germany*
[2]*Institut für Anorganische und Analytische Chemie, Freie Universität Berlin, Fabeckstraße 34-36, D-14195 Berlin-Dahlem, Germany*
(Received 15 October 1996)

We report on a high-resolution photoabsorption study of SiH_4 and SiD_4 in the excitation region below the Si $2p$ threshold. The spectra can be separated into a lower region from valence excitations and an upper region from Rydberg excitations. In the valence region, intense excitations of vibrational bending modes were observed, reflecting a deviation of the core-excited molecules from the T_d symmetry of ground-state silane. The derived geometry of the core- to -valence-excited molecules was found to be similar to that of the equivalent-cores molecule PH_4. For excitations to higher Rydberg states, symmetric-stretching vibrational modes were exclusively observed, while for the lowest Rydberg states, additional bending-mode vibrational excitations were found to contribute. The latter observation can be explained by a mixing of Rydberg and valence character, causing an increase of the deviation from T_d symmetry with increasing valence character of the core-excited state. The spectral shape of the $2p_{3/2}^{-1}5s$ Rydberg state was analyzed by a four-mode Franck-Condon fit, providing insight into the structure of the core-excited molecule. The high instrumental resolution ($\Delta E = 15$ meV full width at half maximum) allowed the derivation of the natural widths Γ of the Rydberg states, which were found to be identical within the limits of error (with $\Gamma = 50 \pm 5$ meV). [S1050-2947(97)02207-5]

PACS number(s): 33.15.Dj, 33.70.Ca, 33.20.Tp, 33.80.Eh

I. INTRODUCTION

Considerable improvements in the resolution of monochromators in the soft-x-ray region in the past decade have resulted in photoabsorption spectra of core-excited molecules with resolved vibrational splittings [1–3]. A number of vibrationally resolved photoabsorption spectra have been reported, including those of the tetrahedral molecules CH_4, CD_4 [4,5], SiH_4, SiD_4 [6–8], SiF_4, [9], and $SiCl_4$ [10]. In all of these cases, only one vibrational mode, the *symmetric-stretching* mode, was found to contribute to the higher Rydberg excitations, while the lowest Rydberg resonances in the spectra of CH_4, CD_4, SiH_4, SiD_4, and SiF_4 exhibited additional *nonsymmetric* vibrational modes. In earlier studies of SiH_4 and SiD_4 there have been some hints to a restriction of the nonsymmetric vibrations to the lowest Rydberg states [6–8], but it could not been clarified whether the nonsymmetric vibrations were really missing or just have not been resolved in the spectral features from excitations to higher Rydberg states.

In this paper, we present vibrationally resolved Si $2p$ photoabsorption spectra of SiH_4 and SiD_4 for both the valence and the Rydberg excitation regions. We find strong excitations of the symmetric-stretching mode in the case of Rydberg states, while additional vibrational modes are observed only in the case of excitations to valence orbitals or to the lowest ns Rydberg states. The occurrence of nonsymmetric vibrational modes in the core-excitation spectra of highly symmetric molecules can be understood on the basis of a lowering of the molecular symmetry upon core excitation. We present a model following the lines of the valence-shell electron-pair repulsion (VSEPR) theory of Gillespie [11] to explain this symmetry lowering. The Si $2p_{3/2}^{-1}5s$ state is found to be a mixed state and the observed spectral envelope is treated by a multimode Franck-Condon analysis, resulting in the molecular parameters of the excited state, i.e., equilibrium distances and angular distortions.

II. EXPERIMENTAL DETAILS

The experiments were performed with the high-resolution SX700/II monochromator, operated by the Freie Universität Berlin at the Berliner Elektronenspeicherring für Synchrotronstrahlung (BESSY). This monochromator includes a plane premirror and a plane grating, a fixed ellipsoidal focusing mirror, and a fixed curved exit slit. Using a 2442-lines/mm grating and a 3-μm exit slit, a resolution of $\cong 15$ meV [full width at half maximum (FWHM)] at $h\nu = 110$ eV can be achieved [12]. The photoabsorption spectra were recorded with a gas-ionization cell 10 cm in active length by monitoring the total photoionization current as a function of photon energy. The gas cell, filled typically with 0.1 mbar of SiH_4 or SiD_4, was separated from the ultrahigh vacuum of the monochromator by a 1200-Å-thick carbon window. The photon energy was calibrated by monitoring the N $1s \rightarrow \pi^*(v''=0 \rightarrow v'=0)$ excitation in gas-phase N_2 at $h\nu = 400.88$ eV [13].

SiH_4 and SiD_4 were synthesized by the reaction of $SiCl_4$ with $LiAlH_4$ and $LiAlD_4$, respectively [14]. The reaction products were purified and analyzed for impurities by infrared (IR) spectroscopy as well as by the absence of photoionization signals in the regions of the C $1s$, N $1s$, and O $1s$ absorption thresholds. In the IR spectrum of SiH_4, only the vibrational modes of SiH_4 were observed. In SiD_4, additional weak spectral features were found, originating from isotopically mixed SiD_3H, due to the finite isotopic purity of the starting material ($LiAlD_4$, enriched to 98%).

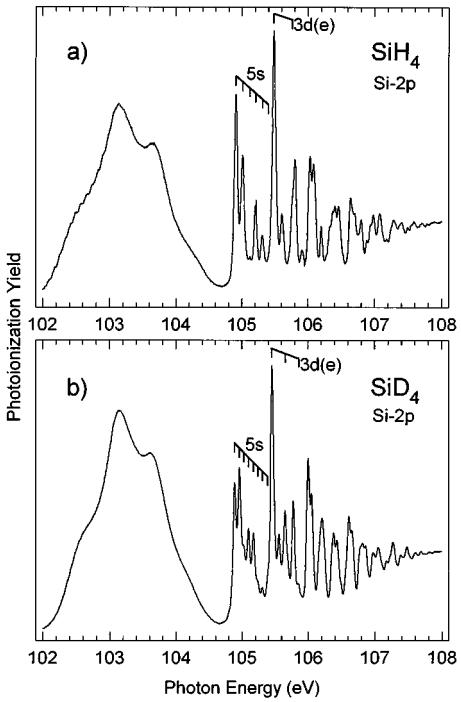

FIG. 1. Overview of the Si $2p$ photoabsorption spectra of gas-phase silane: (a) SiH_4 and (b) SiD_4. The lowest Rydberg states $2p_{3/2}^{-1}5s$ and $2p_{3/2}^{-1}3d(e)$ and their vibrational sidebands are marked by vertical-bar diagrams. In the case of the $2p_{3/2}^{-1}3d(e)$ Rydberg state, excitations of the symmetric-stretching vibrational mode are exclusively observed, whereas the $2p_{3/2}^{-1}5s$ state exhibits additional excitations of bending-mode vibrations.

III. PHOTOABSORPTION SPECTRA OF SILANE MOLECULES

In Fig. 1, the photoabsorption spectra of SiH_4 and SiD_4 below the Si $2p$ ionization threshold are displayed. For both molecules, the spectra can be separated into two different regions. Below 104.7 eV, broad features are observed, originating from excitations to unoccupied antibonding valence orbitals (σ^*). Above 104.7 eV, the spectral features are much narrower and are caused by Si $2p$ excitations to Rydberg states. Such a classification is typical for the second-row hydride molecules HCl [7,15,16], H_2S [7,17], PH_3 [7], and SiH_4 [6–8].

In addition to Rydberg excitations between the lowest vibrational substates ($v''=0\rightarrow v'=0$), a great number of vibrational substates are observed, assigned to excitations from the electronic ground state $v''=0$ to vibrational substates of the electronically excited state $v'=1,2,3,\ldots$. In the case of vibrational energy splittings, the values differ by $\cong\sqrt{2}$ due to the masses of H and D.

The lowest Rydberg states are marked by $5s$ and $3d(e)$ in the spectra of Fig. 1. Typical vibrational substates are marked by the vertical-bar diagrams, with the vibrational energy of the $3d(e)$ state of SiH_4 (SiD_4) being $\cong 300$ meV ($\cong 210$ meV). Vibrational excitations of much lower energies were resolved in the $5s$ Rydberg region, originating obviously from additional vibrational modes. These vibrational modes can be assigned by a comparison of the observed vibrational splittings with those of the electronic ground state of silane. In a five-atom molecule with tetrahedral symmetry, four normal vibrational modes contribute: the symmetric stretching mode with a_1 symmetry, ω_1; the symmetric bending mode with e symmetry ω_2; the asymmetric stretching mode with t_2 symmetry, ω_3; and the asymmetric bending mode with t_2 symmetry, ω_4. For the electronic ground state of SiH_4 (SiD_4), the vibrational energies are known: $\hbar\omega_1''=271.129$ meV (193.8 meV), $\hbar\omega_2''=120.38$ meV (84.95 meV), $\hbar\omega_3''=271.417$ meV (198.177 meV), and $\hbar\omega_4''=113.25$ meV (83.6 meV) [18]. Hence the 300-meV (210-meV) vibrational splitting of the $3d(e)$ state of SiH_4 (SiD_4) can be assigned to the symmetric-stretching mode ω_1 (and possibly also to ω_3). Both stretching (ω_1,ω_3) and bending modes (ω_2,ω_4) are observed in the $5s$ Rydberg resonance.

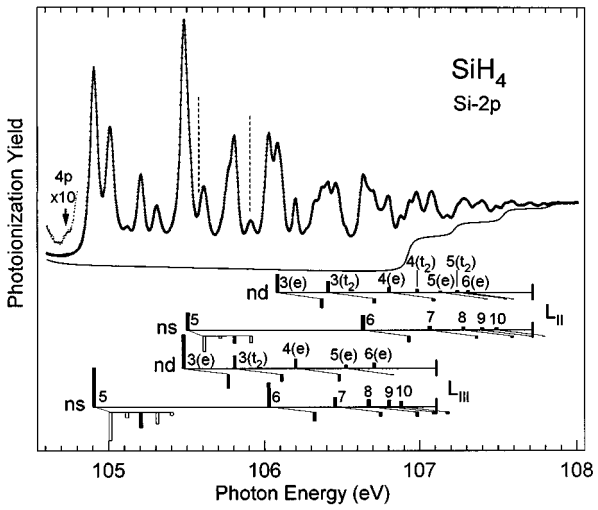

FIG. 2. Rydberg region of the core-excitation spectrum of SiH_4 below the Si $2p$ ionization threshold. The four bar diagrams represent the results of a least-squares-fit analysis. The vertical bars *above* the horizontal lines represent Rydberg excitations between vibrational ground states ($v''=0\rightarrow v'=0$), while those *below* represent excitations to higher vibrational substates. The solid (open) bars mark vibrational excitations of the symmetric-stretching (bending) modes. The lengths of the bars represent the spectral intensities of the resonances. The vertical dashed lines mark the *expected* energies of the missing bending vibrations $3d(e)+\omega_2/\omega_4$ and $3d(t_2)+\omega_2/\omega_4$.

IV. RYDBERG REGION OF THE CORE-EXCITATION SPECTRA OF SiH_4 AND SiD_4

A. Assignment of spectral features

The Rydberg regions of the silane spectra are shown in Figs. 2 and 3. These spectra are similar to those in Refs. [6–8], but they are considerably improved in resolution and signal-to-noise ratio, displaying a substantial number of additional structures. The solid curves through the data points and the vertical bar diagrams represent the results of least-squares-fit analyses. Three Rydberg series, $2p^{-1}ns$, $2p^{-1}nd(e)$, and $2p^{-1}nd(t_2)$, can be identified, converging towards the ionization thresholds L_{III} ($2p_{3/2}^{-1}$) and L_{II} ($2p_{1/2}^{-1}$). Different from the isoelectronic molecules HCl and H_2S [17,19,20], a ligand-field splitting of the $2p_{3/2}^{-1}$ threshold is not observed in silane, in agreement with its tetrahedral

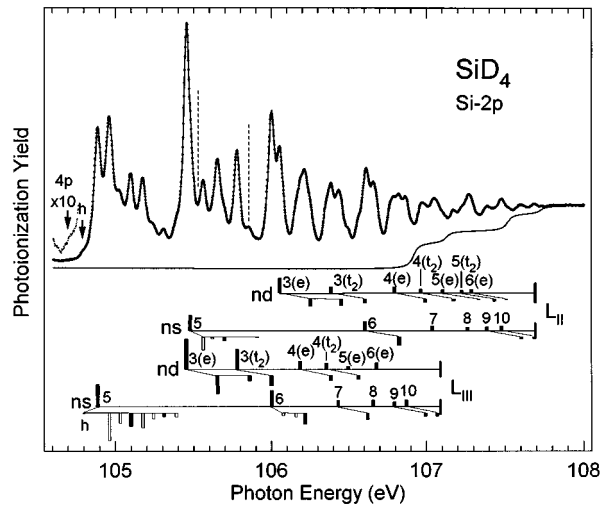

FIG. 3. Rydberg region of SiD_4 below the Si $2p$ ionization threshold. For an explanation, see the caption of Fig. 2. The arrow h at 104.8 eV marks a spectral feature from a hot band: $v''(\omega_4)=1\rightarrow v'=0$.

symmetry. Excitations to Rydberg states with $v'=0$ are marked by vertical bars *above* the horizontal lines in the bar diagrams, while those to higher vibrational substates with $v'=1,2,\ldots$ are marked by vertical bars *below* the horizontal lines. The nd Rydberg series splits into $nd(e)$ and $nd(t_2)$ series, due to the tetrahedral symmetry of the ionic core, which removes the degeneracy of spherical symmetry. For all Rydberg excitations, vibrational substates arising from the symmetric-stretching mode ω_1 are observed, and these are marked by solid vertical bars below the horizontal lines. The $2p_{3/2}^{-1}5s$ and $2p_{1/2}^{-1}5s$ states exhibit additional strong excitations of the vibrational bending modes ω_2 and ω_4; these features are marked by open vertical bars below the horizontal lines. Some very weak bending-mode vibrations are also visible in the $2p_{3/2}^{-1}6s$ resonance of *deuterated* silane. In all other resonances, these bending modes are missing, e.g., in the $2p_{3/2}^{-1}3d(e)$ and $2p_{3/2}^{-1}3d(t_2)$ Rydberg states. The vertical dashed lines in the spectra of SiH_4 and SiD_4 (Figs. 2 and 3) mark the *expected* energies of these bending modes, and it can be seen that these modes are completely missing or are at least very weak. This is obvious since the peak intensities in the bar diagram of Fig. 2 [Fig. 3] can be assigned unequivocally to the $2p_{1/2}^{-1}5s$ bending [$2p_{3/2}^{-1}3d(e)$ stretching] vibrational mode.

Contrary to Sutherland *et al.* [8], but in accordance with Hayes, Brown, and Kunz [6,7], we could not observe a resonance at $h\nu\cong 104.6$ eV (see Fig. 1) that had been quite intense and broad in the spectrum of Ref. [8]. This additional structure might have been caused by impurities. Instead, we resolve two *very* weak features in this energy region, which were assigned to $2p_{3/2}^{-1}4p$ states in the spectra of both SiH_4 and SiD_4. The energy as well as the rather low intensity of the $4p$ Rydberg resonance are in conformity with predictions by Friedrich *et al.* [21] and confirm the theoretically predicted sequence $4p$, $5s$, and $3d(e)$ for the lowest Rydberg states [21–23]. In the SiD_4 spectrum, we also observe an excitation from higher vibrational states of the electronic ground state, i.e., a ''hot band,'' which can be assigned, on the basis of the Franck-Condon analysis presented in Sec. VI, to an excitation from an asymmetric-bending-mode vibrational state in the ground state to the vibrational ground state of the $5s$ Rydberg state, i.e., to a $v''(\omega_4)=1\rightarrow v'=0$ excitation.

For a detailed analysis of the spectra, a least-squares fit was performed, resulting in energies, natural widths Γ, and intensities for all resonances. In this fit analysis, the resonances were described by Voigt profiles, i.e., Lorentzians convoluted by a Gaussian to simulate the spectrometer function. All well-resolved resonance lines were fitted with similar intrinsic widths resulting in $\Gamma\cong 50$ meV, with a scatter of less than ± 5 meV; in the analysis of the less-resolved or weaker resonances, this Γ value was adopted and kept constant. The background was simulated by a superposition of arctan functions, which describe contributions from excitations to continuum states and to unresolved higher Rydberg states (with $n>10$ for s states and $n>6$ for d states). In each spectrum, four arctan functions were superposed, i.e., for the $2p_{3/2}^{-1}$ and $2p_{1/2}^{-1}$ continua of the ionic states without vibrational excitations as well as for the $2p_{3/2}^{-1}$ and $2p_{1/2}^{-1}$ continua of the $v''=0\rightarrow v'=1$ vibrational excitations. The energies are summarized in Table I. In addition to the ns and nd series, a few resonances were found, which can be assigned to $4p$ and $4f$ states.

On the basis of the given assignments and the application of the Rydberg formula $E=I_p-\mathcal{R}/(n-\delta)^2$, with I_p the ionization threshold, $\mathcal{R}$ the Rydberg constant (13.605 eV), and δ the quantum defect, the L_{III} and L_{II} ionization thresholds of SiH_4 (SiD_4) were obtained from the ns and nd Rydberg series as 107.110 ± 0.010 eV (107.090 ± 0.010 eV) and 107.720 ± 0.010 eV (107.695 ± 0.010 eV), respectively. A difference of $\cong 25$ meV in the ionization thresholds of SiH_4 and SiD_4 is visible for each well-resolved Rydberg state, which can be understood by comparing the zero-point vibrational energies in the electronic ground and excited states of SiH_4 and SiD_4 [24]. Note that the energies of the $2p$ ionization thresholds obtained in the present work are $\cong 200$ meV smaller than those derived from photoelectron spectra [25–28]. This difference is apparently not caused by an inaccurate energy calibration since the binding energy of the Kr $3d_{5/2}$ core level found in Ref. [26] ($E_B=93.798$ eV) agrees very well with the Kr $3d_{5/2}$ ionization threshold derived by our group from the $3d_{5/2}^{-1}np$ series (93.786 ± 0.015 eV) [12].

On the basis of the present threshold energies, the quantum defects δ for the s, $d(e)$, and $d(t_2)$ series were derived as 2.45 ± 0.07, 0.15 ± 0.05, and -0.30 ± 0.10, respectively, and that of the weak $4p$ ($4f$) resonance as $\delta=1.60\pm 0.05$ (-0.04 ± 0.02). The quantum defect for the s series is based on the assignment of the 104.9-eV Rydberg resonance to a $5s$ excitation. The derived quantum defects are also close to theoretical values obtained by Schwarz [22], $\delta=2.15$, 0.1, -0.4, and 1.5 for the $5s$, $3d(e)$, $3d(t_2)$, and $4p$ Rydberg states, respectively.

The vibrational energies of the symmetric-stretching mode in SiH_4 (SiD_4) are obtained from the fitting procedure as 297 ± 7 meV (210 ± 10 meV), differing by a factor of $\sqrt{2}$. These values agree very well with previous results from photoabsorption [8] and photoemission [25–28]. The vibrational sidebands were found to be stronger in SiD_4 than in

TABLE I. Energies of Rydberg states and vibrational substates in the Si $2p$ core-excitation spectra of SiH_4 and SiD_4, as obtained from least-squares-fit analyses. For Rydberg excitations between vibrational ground states ($v''=0\rightarrow v'=0$), the quantum defect δ is also given. The error bars for the energies are estimated as ± 5 meV.

	SiH_4				SiD_4			
Excited	$2p_{3/2}^{-1}$		$2p_{1/2}^{-1}$		$2p_{3/2}^{-1}$		$2p_{1/2}^{-1}$	
state	E (eV)	δ	E (eV)	δ	E (eV)	δ	E (eV)	δ
$4p$	104.735	1.61			104.710	1.61		
$5s$ + hot band					104.800			
$5s$	104.909	2.51	105.507	2.52	104.888	2.51	105.478	2.52
$5s+\omega_4/\omega_2$	105.013		105.613		104.963		105.562	
$5s+2\omega_4$	105.119		105.716		105.031		105.621	
$5s+\omega_1$	105.207		105.808		105.099		105.698	
$5s+\omega_1+\omega_4$	105.311		105.914		105.175			
$5s+\omega_1+2\omega_4$	105.403				105.243			
$5s+2\omega_1$					105.309		105.910	
$5s+2\omega_1+\omega_4$					105.388			
$6s$	106.001	2.46	106.637	2.46	106.001	2.47	106.605	2.47
$6s+\omega_4$					106.077			
$6s+2\omega_4$					106.159			
$6s+\omega_1$	106.327		106.933		106.218		106.827	
$7s$	106.458	2.43	107.066	2.44	106.431	2.46	107.039	2.45
$7s+\omega_1$	106.750		107.365		106.622			
$8s$	106.678	2.41	107.281	2.43	106.658	2.39	107.265	2.38
$8s+\omega_1$	106.985		107.592					
$9s$	106.806	2.31	107.400	2.48	106.795	2.21	107.387	2.36
$9s+\omega_1$	107.091		107.704		106.994		107.606	
$10s$	106.881	2.29	107.492	2.28	106.870	2.14	107.480	2.05
$10s+\omega_1$	107.180		107.791		107.068		107.687	
$3d(e)$	105.480	0.11	106.084	0.12	105.453	0.12	106.055	0.12
$3d(e)+\omega_1$	105.766		106.371		105.658		106.253	
$3d(e)+2\omega_1$					105.860		106.453	
$4d(e)$	106.203	0.13	106.806	0.14	106.187	0.12	106.795	0.11
$4d(e)+\omega_1$	106.484		107.091				106.994	
$5d(e)$	106.529	0.16	107.133	0.19	106.498	0.21	107.105	0.20
$5d(e)+\omega_1$	106.829		107.424				107.335	
$6d(e)$	106.709	0.17	106.311	0.23	106.682	0.23	107.289	0.21
$6d(e)+\omega_1$			106.592		106.901		107.511	
$3d(t_2)$	105.808	-0.23	106.411	-0.22	105.779	-0.22	106.387	-0.23
$3d(t_2)+\omega_1$	106.113		106.709		106.001		106.605	
$4d(t_2)$			106.985	-0.30	106.356	-0.31	106.965	-0.32
$4d(t_2)+\omega_1$					106.564		107.175	
$5d(t_2)$			107.243	-0.34			107.226	-0.39
$5d(t_2)+\omega_1$			107.546				107.434	
$6d(t_2)$	106.779	-0.41			106.769	-0.51		
$4f$	106.271	-0.03	106.881	-0.03			106.870	-0.06
$4f+\omega_1$	106.574		107.180				107.068	

SiH_4, particularly in the case of the bending modes of the $2p_{3/2}^{-1}5s$ transition. This is also due to the different masses of H and D and does not reflect differences in the geometries of the excited states (see Franck-Condon analysis in Sec. VI).

B. Natural widths

The least-squares-fit analyses of all well-resolved resonances in the spectra of SiH_4 and SiD_4 result in a natural width of $\Gamma=50\pm5$ meV (FWHM). This value agrees with previous photoemission results by Bozek *et al.* [25], who derived $\Gamma\cong45$ meV with a spectral resolution of $\cong95$ meV, as well as photoabsorption results by Hayes and Brown [7], who obtained a total linewidth (FWHM) of $\cong60$ meV with a spectral resolution of $\cong40$ meV. In the present study, the instrumental resolution is $\cong15$ meV (FWHM), i.e., small compared to the natural width. As a consequence, the present value for the natural width should

be more reliable and more accurate than previous results. Note that the present value of $\Gamma = 50 \pm 5$ meV is larger than the width predicted by theory, $\Gamma^{\text{th}} = 32$ meV [29]. In Ref. [29] the natural widths were calculated for core-ionized states and it was argued that these values might increase by up to 20% for resonantly excited states [30]; nevertheless, this would not be sufficient to resolve the substantial discrepancies between experiment and theory.

C. Symmetry considerations

For the high-n Rydberg states, only the symmetric-stretching vibrational mode was observed, indicating that the molecular structures of these states have T_d symmetry. The tetrahedral symmetry of the high-n Rydberg states can be understood by regarding these core-excited states as ionic SiH_4^+ (SiD_4^+), with the highly excited electron in the ionic potential. The excited electron will not influence the core and the structure of the molecule is therefore identical to that of the corresponding ion. The structures of both the core-ionized SiH_4^+ (SiD_4^+) and the valence-ionized $(Z+1)$ molecule PH_4^+ (PD_4^+) are known to have tetrahedral symmetry [31,32]. From this tetrahedral symmetry it becomes clear why first-order Jahn-Teller distortions due to the triply degenerate $2p$ core hole remain small, in agreement with calculations [31], despite the T_2 symmetry of the total electronic wave function of the ion.

V. VALENCE REGION OF THE Si $2p$ CORE-EXCITATION SPECTRA OF SiH_4 AND SiD_4

The Si $2p$ to valence-orbital excitation region is shown in more detail in Fig. 4. Two resonances split by a spin-orbit interaction are observed in both SiH_4 and SiD_4, assigned to Si $2p^{-1}4a_1$ and Si $2p^{-1}3t_2$ core-excited states. An unambiguous assignment of the two states is not straightforward, however, since the theoretical results contradict each other with respect to valence-orbital sequence and intensity ratio of the Si $2p^{-1}4a_1$ and Si $2p^{-1}3t_2$ excitations. We argue that the configuration-interaction calculations of Friedrich *et al.* [21] describe the intensities and energies of the lowest Rydberg orbitals rather well (see Sec. IV) and we adopt the valence-orbital sequence $4a_1$ and $3t_2$ given by these authors. This sequence has also been given in Refs. [22, 23, 33], whereas Ref. [34] proposed a different sequence that is rejected.

In the valence-orbital region of the SiH_4 spectrum [Fig. 4(a)], a vibrational fine structure with an energy splitting of $\hbar\omega = 83$ meV is clearly visible in the photon-energy region from 102 to 103 eV. In the analogous region of the SiD_4 spectrum [Fig. 4(b)], only a weak vibrational fine structure is found, with $\hbar\omega = 57$ meV. The ratio of vibrational energies for SiH_4 and SiD_4 is found to be $\hbar\omega_{\text{H}}/\hbar\omega_{\text{D}} = 1.46$, i.e., close to the expected value of $\sqrt{2}$. Note that the vibrational energies obtained experimentally for the valence-orbital region are smaller than the lowest vibrations in the ground state, $\hbar\omega_2$ and $\hbar\omega_4$ (bending modes); they are consequently considered to represent bending-vibrational modes.

For the core to σ^* excitations of most of the hydrogen-containing molecules (HBr [35], HCl [36], H_2S [37,38], and SiH_4 [39]), fast dissociation processes have been observed.

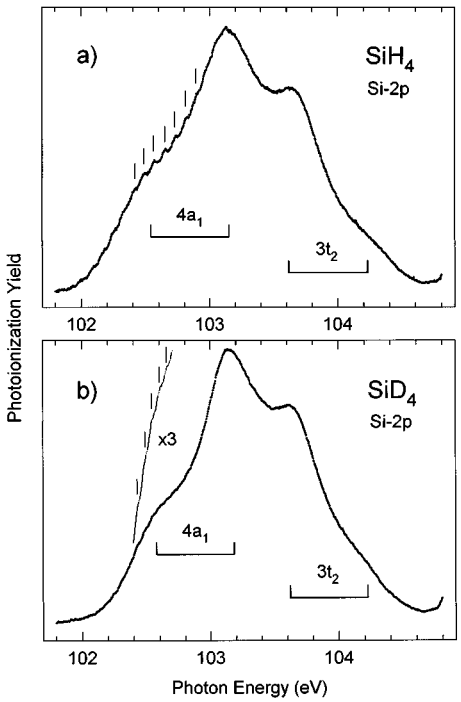

FIG. 4. Valence-orbital region of the Si $2p$ core-excitation spectra of silane: (a) SiH_4, with clearly resolved vibrational fine structure in the 102–103 eV region, and (b) SiD_4, with weak vibrational substates marked by vertical bars in the spectral region enhanced by a factor of 3.

Therefore, the vibrational fine structures observed for the silane molecules are quite astonishing since they require a potential-energy surface of the excited state that is stable with respect to dissociation. However, it had been shown for the case of HCl [36], which is isoelectronic to silane, that a minimum of the potential-energy surface exists even though a fast dissociation process occurs. This is due to changes in the equilibrium distances upon excitation that shift the potential-energy curve *above* the dissociation level.

In the case of SiH_4, de Souza, Morin, and Nenner [39] observed the nondissociated silane molecule as well as dissociation products upon a core to σ^* excitation. They explained their observation by a fast dissociation process along a SiH_3-H coordinate and proposed a schematic potential-energy curve without any barrier along this coordinate. However, in silane the σ^* valence excitations consist of the $4a_1$ and $3t_2$ orbitals, with $3t_2$ split in the case of a deformation along the SiH_3-H coordinate into a_1 and e; i.e., there are three different states. Yavna *et al.* [40] calculated the potential-energy surfaces along the normal coordinates and found that two of the three states ought to be stable. At least one of the states originating from $3t_2$ leads to a fast dissociation, explaining the experimental results of de Souza, Morin, and Nenner. We therefore conclude that the lowest core to valence excitation $2p^{-1}4a_1$ should be stable against dissociation with the Franck-Condon limits of this excitation below the dissociation threshold. This stability of the $2p^{-1}4a_1$ state agrees also with the stability of the equivalent cores molecule PH_4 in the electronic ground state [41].

Note that the vibrational fine structure in the valence orbital region has been observed before by Hudson *et al.* in

H_2S and D_2S [17]. Here, however, the fine structure does not occur in the lowest but in the second state and has been explained by vibronic coupling due to an avoided level crossing within the Franck-Condon limits [37,38].

To further understand the bending-mode vibrations of the $2p^{-1}4a_1$ state, we consider the $Z+1$ molecule PH_4 in the electronic ground state. Most interestingly, the ground state of the PH_4 molecule has been found, on the basis of calculations, to possess an unusual geometry, namely, a C_{2v} symmetry [42–45], as compared to a T_d symmetry; the C_{2v} symmetry allows a stronger deviation of the bending-mode normal coordinates (i.e., angles) than the stretching mode normal coordinates (i.e., distances). Howell and Olsen [42] refer to this geometry with C_{2v} symmetry as the second-order Jahn-Teller effect, which can be understood by correspondence with the VSEPR theory [46]: In addition to the eight bonding electrons, there is a ninth valence electron in a nonbonding orbital, which is located at the so-called equatorial site of the distorted trigonal-bipyramid. This distorts the molecule by a repulsion of the bonding electrons, enlarging the angle between two ligand atoms. If this is also valid for the $2p^{-1}4a_1$ state in silane, which ought to have C_{2v} symmetry, there will be substantial changes of the angles in the T_d symmetry of the electronic ground state. This explains the strong excitation of bending-mode vibrations; if the changes of the distances are minor, we find by simulation that the stretching-mode vibrations will be too weak to be observed in the case of strong angular distortions.

In the following, we argue that a first-order or normal Jahn-Teller effect is negligible for the $2p^{-1}4a_1$ state. The total electronic wave function of this state has T_2 symmetry, i.e., it is degenerate, and a first-order Jahn-Teller effect may therefore contribute, leading to a deformation of the molecule. Nevertheless, we assume that a first-order Jahn-Teller effect is negligible in this case since (i) by neglecting the core hole the excited state cannot undergo a first-order Jahn-Teller effect due to the orbital a_1 symmetry and (ii) by neglecting the excited electron the core hole will also not undergo a first-order Jahn-Teller effect (see Sec. IV C). As a consequence, only an interaction between the core hole and the excited electron could lead to a first-order Jahn-Teller effect; however, the interaction of the localized core hole and the quite *distant* excited electron is expected to be small. In the $Z+1$ model, we conclude for the $2p^{-1}4a_1$ state in silane that the second-order Jahn-Teller effect (equal to the VSEPR mechanism) is substantially larger than a possible first-order Jahn-Teller effect.

VI. FRANCK-CONDON ANALYSIS OF THE "MIXED" 5s STATE

A. The a_1 vibrational modes

Figure 5 displays the core-excitation spectra of SiH_4 and SiD_4 in the region of the $2p_{3/2}^{-1}5s$ state and the $v''=0\rightarrow v'=0$ excitation of the $2p_{3/2}^{-1}3d(e)$ state in more detail. The $2p_{3/2}^{-1}5s$ states were treated by a multimode Franck-Condon curve-fitting procedure, with the results given by the solid lines through the data points. This fit procedure is based on an algorithm first described by Hutchisson [47,48] that provides insight into the molecular geometry of the core-excited

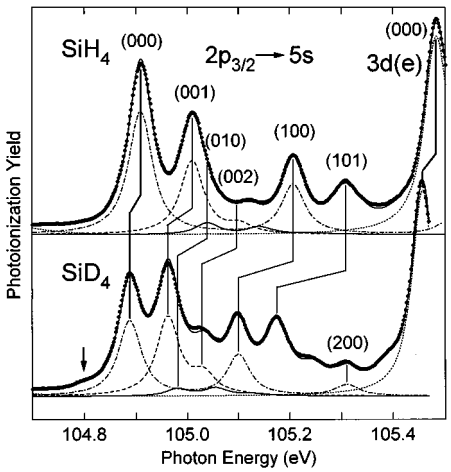

FIG. 5. Core-excitation spectra of SiH_4 and SiD_4 in the region of the $2p_{3/2}^{-1}5s$ and $2p_{3/2}^{-1}3d(e)$ resonances, with resolved vibrational fine structure of the $2p_{3/2}^{-1}5s$ state. The solid lines through the data points represent the results of a three-dimensional Franck-Condon analysis. The most intense vibrational substates are marked by the vibrational quantum numbers (nkl) of the normal-vibrational modes $\omega_1,\omega_2,\omega_4$. The dash-dotted subspectra represent the vibrational substate (000),(100),(200), i.e., $v'=0,1,2$ of $\hbar\omega_1$; the dashed subspectra represent (001),(002), etc., i.e., $v'=1,2,\ldots$ of $\hbar\omega_4$; the solid subspectra represent (010),(011),(020), i.e., $v'=1,2$ of $\hbar\omega_2$ and $v'=1$ of $\hbar\omega_2+\hbar\omega_4$. In a fit of the weak ω_2 substate in the spectrum of SiD_4, $\hbar\omega_2(SiD_4)=\hbar\omega_2(SiH_4)/\sqrt{2}$ was assumed. For SiD_4, a weak feature from a hot band $[v''=(001)\rightarrow v'=(000)]$ is visible; it has been marked by the vertical arrow. For the 25-meV isotope shift between the $v''=(000)\rightarrow v'=(000)$ excitations in SiH_4 and SiD_4, see the text and Ref. [24].

state. We assume that Morse potentials with asymmetries $x_{ii}=(x\hbar\omega)_i$ apply, i.e., the modes were treated as uncoupled.

Various vibrational modes are resolved in the spectra, which can be assigned to the symmetric stretching mode ω_1, the symmetric bending mode ω_2, and the asymmetric bending mode ω_4. In a T_d molecule, these modes have a_1, e, and t_2 symmetry, respectively; the asymmetric stretching mode ω_3 was not observed in the spectra. The vibrational substates are marked by $(nkl)\equiv(\omega_1\omega_2\omega_4)$ in Fig. 5.

In a single-photon photoionization spectrum, only the excitation of vibrational modes with a_1 symmetry is optically allowed. We therefore have to conclude that the observed excitations of the ω_2 and ω_4 modes are caused by a symmetry of the excited state lower than T_d. This causes a splitting of the degenerate modes with e and t_2 symmetry into additional modes with a_1 symmetry. On the basis of arguments given in Sec. V for the valence-orbital region, we assume a C_{2v} symmetry also for the 5s Rydberg state. All modes with a_1 symmetry were taken into account in the multimode Franck-Condon analysis.

B. Prerequisites for the Franck-Condon analysis

At this point we give further supportive arguments for the applicability and validity of the applied multimode Franck-Condon analysis of the $2p\rightarrow 5s$ excitation in silane. For this, two requirements must be fulfilled: (i) The total molecular wave function Ψ can be described in the adiabatic approxi-

mation and (ii) the transition has to be allowed on the basis of the dipole selection rules. The first-order and second-order Jahn-Teller effects may lead to deviations from requirement (i), the adiabatic approximation. Although the final state is triply degenerate due to the $2p$ core hole, the first-order Jahn-Teller effect can be neglected by transferring the conclusions reached for the $2p^{-1}4a_1$ state (see Sec. V) to the $2p^{-1}5sa_1$ state. This means that the given distortion of the $2p^{-1}5s$ core-excited state in silane must be due to a second-order Jahn-Teller effect; however, the second-order Jahn-Teller effect ought to be weak, due to the large energy splitting of the $5s$ and $3d$ states, and the adiabatic approximation should still be appropriate [49]. As for requirement (ii), we argue that the electronic part of the transition matrix element should not vanish since the $2p \rightarrow 5s$ transition is dipole allowed in both symmetries T_d and C_{2v}. As a result, the Franck-Condon approximation should be appropriate for describing the $2p \rightarrow 5s$ excitation. In the Franck-Condon analysis, the intensities of the vibrational sideband are determined by Franck-Condon factors. This leaves the problem of finding appropriate vibrational wave functions of the ground state and the excited states.

In simple cases, when the symmetry is not reduced, a harmonic potential with anharmonic terms is used. However, when the symmetry is reduced, more than one minimum in the potential-energy surface of the excited state has to be expected. This has the consequence that in a hypothetical planar geometry of the molecular ground state, an atom that is displaced from the molecular plane in the excited state may assume two image positions due to the double-minimum potential. In the present silane case, there are six possible positions for the lonely electron, which enlarges the H-Si-H angle, and hence six minima will exist in the potential-energy surface. Each of the vibrations will therefore be split into substates, represented by n^+ and n^-. Despite these general aspects, only one of these minima should actually contribute since for the lower vibrational states the time required for a jump from one minimum to the other is supposedly much longer than the mean lifetime of the core-excited state. One can therefore assume that the molecular configuration is localized at one particular minimum. That this is really the case can be seen in the photoionization spectrum of SiD_4 from the high intensity of the $v''=0 \rightarrow v'(\omega_4)=1$ resonance [marked (001) in Fig. 5; see below] and by the energy of the hot-band feature $v''(\omega_4)=1 \rightarrow v'=0$. The vibrational wave function of the $v''(\omega_4)=1$ state has a nonvanishing overlap only with the $v'=0^-$ substrate of the excited state, whereas the $v''=0 \rightarrow v'=0$ excitation populates the 0^+ substate. The energy difference between the hot band and the $v''=0 \rightarrow v'=0$ $2p_{3/2}^{-1}5s$ Rydberg state is 88 meV, i.e., very close to the ω_4'' vibrational splitting in the ground state (83.6 meV [18]). As a consequence, the energy spacing between the 0^+ and 0^- states must be very small, indicating a high potential barrier between the various minima and consequently a rather low inversion rate; the same arguments will apply to at least the $v'=1$ states. Since the molecule is localized in a single minimum and harmonic-oscillator wave functions can be used for the excited state, we can apply the algorithm given by Hutchisson [47,48] for analyzing the low-n vibrational states.

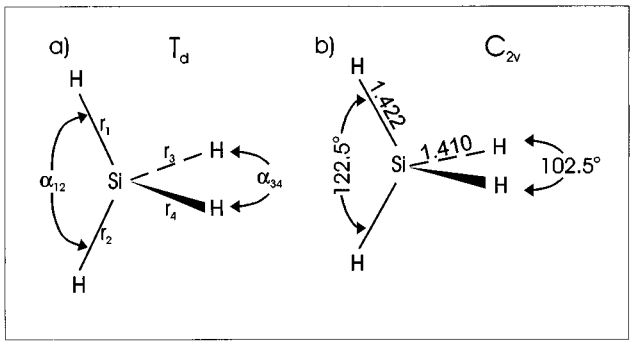

FIG. 6. (a) Definition of intramolecular distances r_1, r_2, r_3, r_4 and angles α_{12}, α_{34} used in the Franck-Condon analysis. (b) Geometry of the core-excited $2p^{-1}5s$ Rydberg state in both SiH_4 and SiD_4, resulting from the Franck-Condon analysis.

In the case of high-n vibrational states above the potential barrier, it might be necessary to start from a harmonic oscillator that contains all minima: Then there will be no change in the normal coordinates upon electronic excitation. The vibrational wave functions will then be approximately orthogonal to the ground-state wave function, resulting in an almost vanishing overlap and hence a quenching of the high-n vibrations. If this would also hold for low-n vibrations, the $v'(\omega_4;\omega_2)=1,2,\ldots$ excitations should not be observed. On the basis of the given arguments, the observed intensities of the higher vibrational substates can be lower than expected in the model of one localized minimum, but these high-n vibrations have essentially no influence on the results of the Franck-Condon analysis. It turns out that the changes of the molecular geometry obtained from the fit represent a lower limit and the correct angular distortions might be $\cong 2°$ larger.

C. Multimode Franck-Condon analysis

On the basis of the three measured vibrational modes ω_i, a multidimensional Franck-Condon analysis was performed by taking the additional normal modes with a_1 symmetry into account. As a result, the excitation-induced changes ΔQ_i of the normal coordinates Q_i were obtained. In order to convert these normal coordinates into geometrical parameters of the molecule, such as intramolecular distances and angles, it is necessary to know the relationship between the normal coordinates, the symmetry coordinates, and the internal coordinates (bonding angles and interatomic distances). This relationship was calculated with the algorithm described by Wilson, Decius, and Cross [50]. In a first step, the internal coordinates were converted to symmetry coordinates, and in a second step, the symmetry coordinates were transformed to normal coordinates.

For a five-atom molecule such as silane, we are dealing with nine normal coordinates Q_i and nine symmetry coordinates S_i. In the C_{2v} molecular symmetry, four of them have a_1 symmetry. In a first step, we define the four symmetry coordinates of silane with a_1 symmetry in the C_{2v} point group by relating them with internal coordinates, i.e., with the distances between the Si atom and the ith H atom r_i and the angle between r_i and r_j, α_{ij} [see Fig. 6(a)]. We define a symmetry-coordinate vector

$\mathcal{S}_i=(S_1,S_2,S_3,S_4)$and an internal-coordinate vector $\mathbf{S}_i=(r_1,r_2,r_3,r_4,\alpha_{12},\alpha_{34},\alpha_{13},\alpha_{14},\alpha_{23},\alpha_{24})$, which are related by the transformation matrix $\mathbf{U}_{ij}$, with $\mathcal{S}_i=\mathbf{U}_{ij}\mathbf{S}_j$. In Ref. [51], $\mathbf{U}_{ij}$ has been given explicitly. The symmetry-coordinate vector $\mathcal{S}_i=(S_1,S_2,S_3,S_4)$ and the normal-coordinate vector $\mathbf{Q}_i=(Q_1,Q_2,Q_3,Q_4)$ are related by a matrix $\mathbf{L}_{ik}$, with

$$\mathcal{S}_i=\mathbf{L}_{ik}\mathbf{Q}_k .$$

In this way, we obtain the following relation between the internal-coordinate vector $\mathbf{S}_j$ and the normal-coordinate vector $\mathbf{Q}_k$:

$$\mathbf{S}_j=\mathbf{U}_{ji}\mathbf{L}_{ik}\mathbf{Q}_k ,$$

with the transposed matrix $\mathbf{U}_{ji}=\mathbf{U}_{ij}^T$. For tetrahedral symmetry of the molecular ground state ($r_i=$const and $\alpha_{ij}=109.47°$), only the off-diagonal elements L_{34} and L_{43} have to be considered and all other $L_{ik}=0$ are valid for $i\neq k$. The following matrix $\mathbf{L}_{ik}$ results:

$$\mathbf{L}_{ik}=\begin{pmatrix} L_{11} & 0 & 0 & 0 \\ 0 & L_{22} & 0 & 0 \\ 0 & 0 & L_{33} & L_{43} \\ 0 & 0 & L_{34} & L_{44} \end{pmatrix} . \tag{1}$$

Any deviation from the tetrahedral geometry of the ground state (all r_i equal and $\alpha_{ij}=109.47°$) gives rise to $L_{ik}\neq 0$ for all i and k, i.e., to normal coordinates that are linear combinations of all four symmetry coordinates. This mixing is assumed to be small and is neglected in the excited state. Consequently, the internal-coordinate vectors of the ground and the excited states are related to the normal-coordinate vector by $\mathbf{S}_j=\mathbf{U}_{ji}\mathbf{L}_{ik}\mathbf{Q}_k=\mathbf{\Lambda}_{jk}\mathbf{Q}_k$:

$$\mathbf{U}_{ji}\mathbf{L}_{ik}\equiv\mathbf{\Lambda}_{jk}=\begin{pmatrix} \frac{1}{2}L_{11} & 0 & \frac{1}{2}L_{33} & \frac{1}{2}L_{43} \\ \frac{1}{2}L_{11} & 0 & \frac{1}{2}L_{33} & \frac{1}{2}L_{43} \\ \frac{1}{2}L_{11} & 0 & -\frac{1}{2}L_{33} & -\frac{1}{2}L_{43} \\ \frac{1}{2}L_{11} & 0 & -\frac{1}{2}L_{33} & -\frac{1}{2}L_{43} \\ 0 & \frac{1}{\sqrt{3}}L_{22} & -\frac{1}{\sqrt{2}}L_{34} & -\frac{1}{\sqrt{2}}L_{44} \\ 0 & \frac{1}{\sqrt{3}}L_{22} & \frac{1}{\sqrt{2}}L_{34} & \frac{1}{\sqrt{2}}L_{44} \\ 0 & -\frac{1}{\sqrt{12}}L_{22} & 0 & 0 \\ 0 & -\frac{1}{\sqrt{12}}L_{22} & 0 & 0 \\ 0 & -\frac{1}{\sqrt{12}}L_{22} & 0 & 0 \\ 0 & -\frac{1}{\sqrt{12}}L_{22} & 0 & 0 \end{pmatrix} . \tag{2}$$

In this way, we obtain $\Delta\mathbf{S}_j=\mathbf{\Lambda}_{jk}\Delta\mathbf{Q}_k$, with $\Delta\mathbf{S}_j=\mathbf{S}_j''-\mathbf{S}_j'$ and $\Delta\mathbf{Q}_k=\mathbf{Q}_k''-\mathbf{Q}_k'$. The double-primed and single-primed entities, respectively, refer to the ground and the excited state.

Applying the procedure of Ref. [52], the elements L_{jk} can be calculated from the force constants F_{ik}, which were taken for silane from the literature [53]. For most sets of force constants, $L_{43}\cong 0$ was obtained leading us to set its value equal to zero. Since a nonvanishing L_{34} will have only a very small influence of less than 0.1° on the angular changes, we have also neglected L_{34}. This reduces the relations obtained from the matrix $\mathbf{\Lambda}_{jk}$ to the following equations between changes of the internal coordinates S_j and those of the normal coordinates Q_k:

$$\Delta r_i=\tfrac{1}{2}L_{11}\Delta Q_1+\tfrac{1}{2}L_{33}\Delta Q_3=\Delta r_i(Q_1)+\Delta r_i(Q_3) \qquad (i=1,2),$$

$$\Delta r_i=\tfrac{1}{2}L_{11}\Delta Q_1-\tfrac{1}{2}L_{33}\Delta Q_3=\Delta r_i(Q_1)+\Delta r_i(Q_3) \qquad (i=3,4),$$

TABLE II. Vibrational energies $\hbar\omega_i'$, anharmonicities $(x\hbar\omega)_i'$, and changes of the geometrical parameters of the core-excited molecules with respect to the ground-state (g.s.) values [18]. The given numbers were derived from changes of the normal coordinates ΔQ_i obtained by Franck-Condon analyses. $\hbar\omega_2'(SiD_4)$ was assumed to be $\hbar\omega_2'(SiH_4)/\sqrt{2}$ and is marked by square brackets. The vibrational energies of the equivalent-cores molecules PH_4^+ and PD_4^+ are included for comparison [54]. For the splitting of the ω_2 and ω_4 modes, see the text. The error bars are given in units of the last digit.

	SiH_4		SiD_4			
Vibrations and geometries	g.s.	$2p_{3/2}^{-1}5s$	g.s.	$2p_{3/2}^{-1}5s$	PH_4^+	PD_4^+
$\hbar\omega_1$ (meV)	271.129	298.5(10)	193.8	212.9(10)	284.5	205.1
$(x\hbar\omega)_1$ (meV)				0.85(5)		
$\Delta r_{1;2;3;4}(Q_1)$ (Å)		$-0.055(1)$		$-0.055(1)$		
$\hbar\omega_2$ (meV)	120.38	131.1(1.0)	84.95	[92.6]	135.5/127.2	96.3/89.9
$\Delta\alpha_{12;34}(Q_2)$ (deg)		3.1(5)		2.7(5)		
$\Delta r_{1;2}(Q_3) = -\Delta r_{3;4}(Q_3)$ (Å)		0.006(6)		0.006(6)		
$\hbar\omega_4$ (meV)	113.25	106.6(1.0)	83.6	78.0(1.0)	118.3/113.9	86.9/83.3
$(x\hbar\omega)_4$ (meV)		3.2(3)		2.3(3)		
$\Delta\alpha_{12}(Q_4) = -\Delta\alpha_{34}(Q_4)$ (deg)		9.6(5)		10.2(5)		

$$\Delta\alpha_{12}=\frac{1}{\sqrt{3}}L_{22}\Delta Q_2-\frac{1}{\sqrt{2}}L_{44}\Delta Q_4=\Delta\alpha_{12}(Q_2)+\Delta\alpha_{12}(Q_4),$$

$$\Delta\alpha_{34}=\frac{1}{\sqrt{3}}L_{22}\Delta Q_2+\frac{1}{\sqrt{2}}L_{44}\Delta Q_4=\Delta\alpha_{34}(Q_2)+\Delta\alpha_{34}(Q_4),$$

$$\Delta\alpha_{ij}=-\frac{1}{\sqrt{12}}L_{22}\Delta Q_2=\Delta\alpha_{ij}(Q_2)\quad(ij=13,14,23,24). \tag{3}$$

D. Results

From the Franck-Condon analysis of the spectra, the three normal vibrational modes of the excited state of SiH_4 (SiD_4) were obtained: $\hbar\omega_1'=298.5$ meV (212.9 meV), $\hbar\omega_2'=131.1$ meV (92.6 meV), and $\hbar\omega_4'=106.6$ meV (78.8 meV). The modes were assigned by comparison with the appropriate $Z+1$ ions PH_4^+ and PD_4^+, for which the vibrational energies are known from studies of PH_4I (PD_4I): $\hbar\omega_1=284.5$ meV (205.06 meV), $\hbar\omega_2=135.5/127.2$ meV (96.3/89.9 meV), $\hbar\omega_3=281.7/293.3$ meV (205.55/214.7 meV), and $\hbar\omega_4=118.3/113.94$ meV (86.9/83.3 meV) [54]. Note that the ω_2, ω_3, and ω_4 values for PH_4^+ (PD_4^+) are split due to the D_{2d} symmetry at the PH_4^+ (PD_4^+) ion in PH_4I (PD_4I); therefore, two values were given in each case. In this way, the ω_2' and ω_4' modes are assigned to bending-vibrational modes, while the ω_1' mode is assigned to the symmetric-stretching mode ω_1, with the possibility of a weak ω_3-mode contribution (see below).

The results of the multimode Franck-Condon analysis are summarized in Table II. They include the vibrational energies $\hbar\omega_i$, the anharmonicities $(x\hbar\omega)_i$, and the contributions $\Delta r_i(Q_k)$ and $\Delta\alpha_{ij}(Q_k)$ of the normal-coordinate changes ΔQ_k to the bond lengths r_i and the bond angles α_{ij}. A geometrical interpretation of the four normal modes ω_i ($i=1,\ldots,4$) is provided by the matrix $\mathbf{\Lambda}_{jk}$, with $L_{34}=L_{43}=0$: ω_1 causes *equal* changes in all bond distances r_i; ω_3 changes the bond distances in a way that $\Delta r_{1;2}=-\Delta r_{3;4}$; ω_2 influences α_{12} and α_{34} in the same way and $\alpha_{13;14;23;24}$ with half the change and the opposite sign; ω_4 changes only α_{12} and α_{34}, with $\Delta\alpha_{12}=-\Delta\alpha_{34}$.

The changes of the internal coordinates upon core excitation are the same for SiH_4 and SiD_4, within the limits of error. This means that the geometries of core-exited SiH_4 and SiD_4 are very similar and the relative intensities of the vibrational sidebands follow from the different masses of the ligand atoms.

Within the four a_1 normal modes, the two bending modes ω_2 and ω_4, representing the angular changes upon core excitation, are well separated in the spectral features. The stretching modes ω_1 and ω_3, however, coincide with a single vibrational energy of 298.5 eV (212.9 eV) for SiH_4 (SiD_4). Consequently, it is simple to separate the effects of angular changes on Q_2 and Q_4, while the effects of bond-length variations on Q_1 and Q_3 overlap considerably. As a consequence, a separation of bond-length variations due to $\Delta r_i(Q_1)$ and $\Delta r_i(Q_3)$ cannot be performed in an unambiguous way.

The excitation of the ω_4' vibrational mode, with $\hbar\omega_4'=106.6$ meV (78.0 meV) for SiH_4 (SiD_4), is caused by a change of the normal coordinate Q_4; it leads to an angular distortion of the molecule given by an increase of α_{12} by $\cong 10°$ and a decrease of α_{34} by the same amount, with all the other angles unchanged. The fit provides also an anharmonicity of the ω_4 vibration of $(x\hbar\omega)_4'=3.2$ meV (2.3 meV) for SiH_4 (SiD_4). These values are comparatively large, but they agree quite well with the ground-state anharmonicity of SiH_4, $(x\hbar\omega)_4''=2$ meV [55]. This observation could also indicate the existence of multiple minima in the potential-energy surface, giving rise to low intensities of the vibrational substates (see Sec. VI B). Note that in the case of constant ΔQ, a high anharmonicity will lead to a low intensity of the higher vibrational substates.

The weak vibrational mode ω_2, with $\hbar\omega_2'=131.1$ meV (92.6 meV) for SiH_4 (SiD_4), is related to a small change of the normal coordinate Q_2 leading to an angular distortion of $|\Delta\alpha_{12;34}(Q_2)|\cong 3°$. Since no anharmonicity could be obtained for this vibrational mode due to the weakness of the

vibrational sidebands, the sign of $\Delta\alpha_{12;34}(Q_2)$ could not be determined. However, if we assume that the Si $2p\rightarrow$ valence excitations are similar to the valence excitations in the $Z+1$ molecule PH_4, we may adopt the positive values $\Delta\alpha_{12;34}(Q_2)\cong+25°$ and $\Delta\alpha_{12}(Q_4)=-\Delta\alpha_{34}(Q_4)\cong+37.5°$ [42]. On the same equivalent-cores basis, we assume that α_{12} and α_{34} increase by 3° and all other angles decrease by 1.5° [see Eq. (3)] due to the change of the normal coordinate Q_2.

The largest vibrational splitting in the SiH_4 (SiD_4) spectrum, $\hbar\omega_1'=298.5$ meV (212.9 meV), is due to the two stretching-vibrational modes. It reflects a decrease of the Si-H(D) equilibrium distance upon core excitation by $\Delta r_i(Q_1)=-0.055\pm0.001$ Å, with supposedly $\Delta r_i(Q_3)=0$. This result agrees very well with recent calculations [31], which obtained a contraction of the silane molecule by 0.05 Å upon core excitation. It also means that the equilibrium distance changes from $r''=1.471$ Å in the ground state [56] to $r'=1.416$ Å in the core-excited state, in good agreement with the bond length of the equivalent-core molecule PH_4^+, $r=1.42\pm0.02$ Å. For SiD_4 an anharmonicity of $(x\hbar\omega)_1'=0.85\pm0.5$ meV is obtained, with the relative large uncertainty caused by the weakness of the $v'=2$ vibration. For SiH_4, an anharmonicity could not be derived due to the disappearance of a $v'=2$ vibration in the $3d(e)$ resonance.

As mentioned before, the symmetric-stretching mode ω_1 may overlap with the asymmetric-stretching mode ω_3, causing a nonvanishing change in Q_3 and hence a nonvanishing $\Delta r_i(Q_3)$. To estimate the ω_1/ω_3 correlation, we performed fits of $\Delta r_i(Q_3)$, with $\Delta r_i(Q_1)$ being varied between -0.055 and 0.0 Å; the results are presented in Fig. 7(a). A small variation of $\Delta r_i(Q_1)$ around -0.055 Å causes obviously a strong increase in $\Delta r_i(Q_3)$. This can be explained by the fact that for one normal coordinate Q the $v'=1$-to-$v'=0$ intensity ratio I_1/I_0 increases very strongly with an increase in $\Delta r_i(Q)$ [see the inset in Fig. 7(a)]. It means that a *small* decrease of $|\Delta r_i(Q_1)|$ at $\Delta r_i(Q_1)=-0.055$ Å will lead to a *strong* decrease of the intensity of the first vibrational substate $v'=1$, which in turn will cause a strong increase of $\Delta r_i(Q_3)$ at $\Delta r_i(Q_3)=0$.

From the results given in Fig. 7(a), we calculated the shorter bond length $r_{3,4}'$ as a function of the longer bond length $r_{1,2}'$. The results, shown in Fig. 7(b), reveal that the shorter bond length $r_{3,4}'$ varies from 1.416 to 1.390 Å and back to 1.416 Å, while the longer bond length $r_{1,2}'$ changes from 1.416 to 1.525 Å. This reflects a redistribution of $Q_1=100\%$ at $r_{1,2}'=1.416$ Å to $Q_3=100\%$ at $r_{1,2}'=1.525$ Å. On the other hand, the shorter P-H bond length r_s in the ground state of various PH_x ($x=3,4,5$) is known to vary slightly under very different molecular conditions with distances $r_s''=1.420$ Å (PH_3, experimental value [57]), $r_s''=1.404$ Å (PH_4, average value of calculations in Refs. [42–45]), $r_s''=1.42$ Å (PH_4^+, experimental value [32]), and $r_s''=1.415$ Å (PH_3, average value of calculations summarized in Ref. [58]). By transferring these small variations of the P-H bond length on the basis of the $Z+1$ approximation to the Si-H bond length of core-excited silane, we expect only a small difference in the bond lengths of core-ionized SiH_4^+ and the short bond length $r_{3,4}'$ of the $2p^{-1}5s$ Rydberg

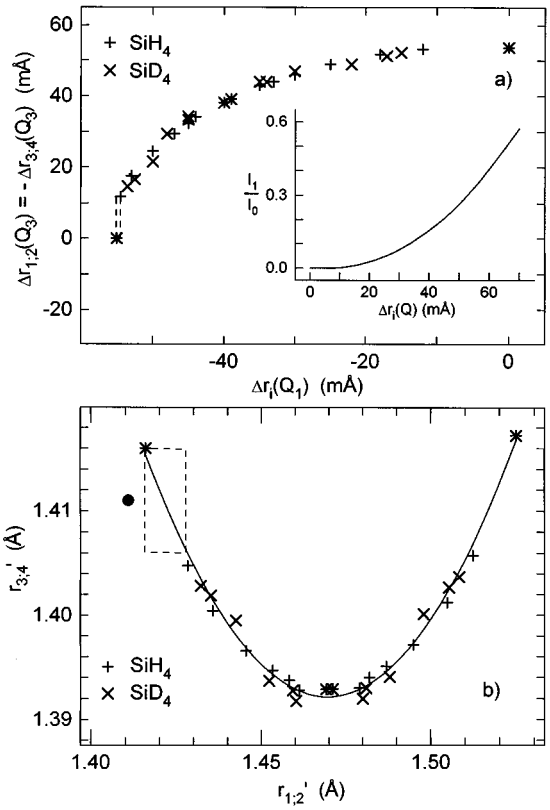

FIG. 7. (a) $\Delta r_i(Q_3)$ as a function of $\Delta r_i(Q_1)$ obtained from a multimode Franck-Condon fit of the $2p_{3/2}^{-1}5s$ excitation spectrum of SiH_4 (+) and SiD_4 (×). The dashed rectangle represents the possible $\Delta r_i(Q_1)$ and $\Delta r_i(Q_3)$ ranges from the results in (b). Note the high uncertainty in $\Delta r_i(Q_3)$. Inset: simulated intensity ratio I_1/I_0 of the $v'=1$ to $v'=0$ sidebands of the stretching modes in SiH_4 as a function of $\Delta r_i(Q)$. (b) Calculated bond distances $r_{1;2}'$ and $r_{3;4}'$ for SiH_4 (+) and SiD_4 (×) on the basis of the results in (a); the solid line represents $r_{1;2}'$ as a function of $r_{3;4}'$. The filled circle represents the geometry of core-ionized SiH_4^+ or SiD_4^+. The possible values for $r_{1;2}'$ and $r_{3;4}'$ are represented by the dashed rectangle. Note that the ordinate and abscissa scales in (a) and (b) differ by factors of 2 and 3, respectively.

state in silane. The two states differ only by a fraction of an additional valence electron that will influence the bond lengths, which leads to an estimate of the difference in bond lengths in SiH_4^+ as compared to the short bond length $r_{3,4}'$ of the $2p^{-1}5s$ Rydberg state of less than 0.005 Å. To estimate the mean $r_{3,4}'$ value, we use Franck-Condon factors for the symmetric-stretching vibrational substates as obtained from photoemission spectra [26,31], assuming $\Delta r_i(Q_3)=0$ Å. We then obtain $\Delta r_i(Q_1)=-0.060$ Å, i.e., $r_1=r_2=r_3=r_4=1.411$ Å, this result is marked by a filled circle in Fig. 7(b). Due to the small fraction of a lonely electron in the $2p^{-1}5s$ state, we estimate a variation of $r_{3;4}$ from 1.406 to 1.416 Å, close to the tetrahedral molecule with $r_{1;2}=1.416-1.428$ Å [see the rectangle in Fig. 7(b)]. This $r_{1;2}/r_{3;4}$ rectangle is transformed to the $\Delta r_i(Q_1)/\Delta r_i(Q_3)$ rectangle in Fig. 7(a). Obviously, $\Delta r_i(Q_1)$ varies by only 0.001 Å, while $\Delta r_i(Q_3)$ varies by 0.012 Å. This means that the Q_1 contribution is constant, $\Delta r_i(Q_1)=-0.055$ Å, while the Q_3 contribution results in $\Delta r_{1;2}=-0.055$ to -0.043 Å

TABLE III. Summary of the internal-coordinate changes in silane (SiD_4 and SiH_4) upon $2p^{-1}5s$ core excitation, separated into the individual contributions $\Delta S_j(Q_k)$. The error bars are given in units of the last digit.

$r'_{1;2}=r''+\Delta r_i(Q_1)+\Delta r_i(Q_3)=1.471\ \text{Å}-0.055(1)\ \text{Å}+0.006(6)\ \text{Å}=1.422(7)\ \text{Å}$
$r'_{3;4}=r''+\Delta r_i(Q_1)+\Delta r_i(Q_3)=1.471\ \text{Å}-0.055(1)\ \text{Å}-0.006(6)\ \text{Å}=1.410(7)\ \text{Å}$
$\alpha'_{12}=\alpha''+\Delta\alpha_{12}(Q_2)+\Delta\alpha_{12}(Q_4)=109.5°+3(0.5)°+10(0.5)°=122.5(1.0)°$
$\alpha'_{34}=\alpha''+\Delta\alpha_{12}(Q_2)+\Delta\alpha_{12}(Q_4)=109.5°+3(0.5)°-10(0.5)°=102.5(1.0)°$
$\alpha'_{13,14,23,24}=\alpha''+\Delta\alpha_{13,14,23,24}(Q_2)=109.5°-1.5(0.5)°=108.0(0.5)°$

and $\Delta r_{3;4}=-0.067$ to -0.055 Å. Note that the I_1/I_0 intensity ratio as a function of $\Delta r_i(Q)$ shows that a fraction of 10% to the (100) vibrational sideband can be considered as an upper limit for $\Delta r_i(Q_3)\cong 0.012$ Å, even though $|\Delta r_i(Q_3)|$ can be as large as 20% of $|\Delta r_i(Q_1)|$.

The changes of the internal coordinates of SiH_4 and SiD_4 upon $Si2p^{-1}5s$ excitation, separated into contributions from the individual normal coordinates, are summarized in Table III. These geometrical changes are also represented in Fig. 6(b).

E. Mixed states

The spectra of the $5s$ Rydberg state reveal excitations of the bending-vibrational mode, however, much weaker than in the valence region. In the case of the $2p_{3/2}^{-1}6s$ Rydberg state, very weak sidebands of this mode could only be observed for SiD_4, but not for SiH_4. These bending vibrations can also be understood on the basis of a distorted T_d symmetry caused by second-order Jahn-Teller effect; this is analogous to a valence-state excitation leading also to C_{2v} symmetry. The bending-vibrational modes can also be understood on the basis of the VSEPR theory if one assumes mixed states, i.e., states with mixed valence and Rydberg character. Such a partial valence character leads to a fraction of a nonbonding ''ninth'' electron in the valence shell and hence to a weaker interaction with the bonding orbitals and a smaller distortion than in a core-valence excitation. The assumption of a mixed state for the $5s$ Rydberg orbital is confirmed by comparing the spectra of gas-phase and condensed silane: Rydberg states are usually quenched in the condensed phase, whereas valence states remain unaffected. In the present case, the condensed-phase spectrum extends from the valence region up to the $5s$ region, supporting our conclusion of a mixed character of this state [21]. The results obtained in the present work are similar to previous results for SiF_4, where the $4s$ Rydberg state had shown additional bending modes confirming a mixed-state character [9].

VII. SUMMARY AND CONCLUSIONS

High-resolution and high-signal-to-noise-ratio photoionization spectra of SiH_4 and SiD_4 were measured in the region of the Si $2p$ core excitations. As compared to previous work [6–8], the improved resolution and higher flux of the SX700/II monochromator at BESSY made it possible to derive a wealth of information from the spectra. Different structures were observed, particularly in the high-n Rydberg region. Bending-vibrational modes could be resolved in the valence-orbital region. Both bending and symmetric-stretching vibrational modes were observed for the $5s$ state, while for higher Rydberg states only the symmetric-stretching vibrations were found. The excitation of bending vibrational modes is due to a deviation from T_d symmetry, i.e., a reduction to C_{2v} symmetry. The valence region gives the largest distortion from T_d symmetry. The $5s$ ''Rydberg'' state was assigned to a mixed state, i.e., a Rydberg state with admixing of valence character, while the high-n Rydberg states were found to be rather pure. The natural widths of the core-excited Rydberg states were found to be equal within the limits of error, with $\Gamma=50\pm5$ meV.

ACKNOWLEDGMENTS

This work was supported by the Bundesminister für Bildung, Wissenschaft, Forschung und Technologie, Project No. 05-650-KEA, and the Deutsche Forschungsgemeinschaft, Project No. DO 561/1-1.

[1] Y. Ma, C. T. Chen, G. Meigs, K. Randall, and F. Sette, Phys. Rev. A **44**, 1848 (1991).
[2] M. Domke, C. Xue, A. Puschmann, T. Mandel, E. Hudson, D. A. Shirley, and G. Kaindl, Chem. Phys. Lett. **173**, 122 (1990); **174**, 668 (1990).
[3] G. Remmers, M. Domke, A. Puschmann, T. Mandel, C. Xue, G. Kaindl, E. Hudson, and D. A. Shirley, Phys. Rev. A **46**, 3935 (1992).
[4] G. Remmers, M. Domke, and G. Kaindl, Phys. Rev. A **47**, 3085 (1993).
[5] K. Ueda, M. Okunsihi, H. Chiba, Y. Shimizu, K. Ohmori, Y. Sato, E. Shigemasa, and N. Kosugi, Chem. Phys. Lett. **236**, 311 (1995).
[6] W. Hayes, F. C. Brown, and A. B. Kunz, Phys. Rev. Lett. **27**, 774 (1971).
[7] W. Hayes and F. C. Brown, Phys. Rev. A **6**, 21 (1972).
[8] D. G. J. Sutherland, G. M. Bancroft, J. D. Bozek, and K. H. Tan, Chem. Phys. Lett. **199**, 341 (1992).
[9] R. Püttner, M. Domke, K. Schulz, and G. Kaindl, Chem. Phys. Lett. **250**, 145 (1996).
[10] M. Domke, R. Püttner, K. Schulz, and G. Kaindl, Phys. Rev. A **52**, 1147 (1995).

[11] R. J. Gillespie, J. Chem. Educ. **40**, 295 (1963).
[12] M. Domke, T. Mandel, A. Puschmann, C. Xue, D. A. Shirley, G. Kaindl, H. Petersen, and P. Kuske, Rev. Sci. Instrum. **63**, 80 (1992).
[13] R. N. S. Sodhi and C. Brion, J. Electron Spectrosc. Relat. Phenom. **34**, 363 (1984).
[14] *Handbuch der Präparativen Anorganischen Chemie*, 3rd ed, edited by G. Brauer (Enke-Verlag, Stuttgart, 1978), p. 654.
[15] D. A. Shaw, D. Cvejanovic, G. C. King, and F. H. Read, J. Phys. B **17**, 1173 (1984).
[16] K. Ninomiya, E. Ishiguro, S. Iwata, A. Mikuni, and T. Sasaki, J. Phys. B **14**, 1777 (1981).
[17] E. Hudson, D. A. Shirley, M. Domke, G. Remmers, and G. Kaindl, Phys. Rev. A **49**, 161 (1994).
[18] *Gmelin Handbook of Inorganic Chemistry, Silicon Suppl. Vol. B 1*, 8th ed., edited by H. Keller-Rudek, D. Koschel, U. Krüerke, and P. Merlet (Springer, Berlin, 1982), p. 94.
[19] S. Svensson, A. Ausmees, S. J. Osborne, G. Bray, F. Gel'mukhanov, H. Ågren, A. Naves de Brito, O.-P. Sairanen, A. Kivimäki, E. Nõmmiste, H. Aksela, and S. Aksela, Phys. Rev. Lett. **72**, 3021 (1994).
[20] H. Aksela, E. Kukk, S. Aksela, O.-P. Sairanen, A. Kivimäki, E. Nõmmiste, A. Ausmees, S. J. Osborne, and S. Svensson, J. Phys. B **28**, 4259 (1995).
[21] H. Friedrich, B. Sonntag, P. Rabe, W. Butcher, and W. H. E. Schwarz, Chem. Phys. Lett. **64**, 360 (1979).
[22] W. H. E. Schwarz, Chem. Phys. **9**, 157 (1975).
[23] W. H. E. Schwarz, Chem. Phys. **11**, 217 (1975).
[24] R. Püttner, M. Domke, D. Lentz, and G. Kaindl, J. Phys. Lett. B **29** L565 (1996).
[25] J. D. Bozek, G. M. Bancroft, J. N. Cutler, and K. H. Tan, Phys. Rev. Lett. **65**, 2757 (1990).
[26] D. G. J. Sutherland, G. M. Bancroft, and K. H. Tan, J. Chem. Phys. **97**, 7918 (1992).
[27] D. G. J. Sutherland, G. M. Bancroft, and K. H. Tan, Surf. Sci. Lett. **262**, L96 (1992).
[28] Z. F. Liu, G. M. Bancroft, J. N. Cutler, D. G. J. Sutherland, J. S. Tse, R. G. Cavell, and K. H. Tan, Phys. Rev. A **46**, 1688 (1992).
[29] J. McColl and F. P. Larkins, Chem. Phys. Lett. **196**, 343 (1992).
[30] F. P. Larkins, Aust. J. Phys. **49**, 457 (1996).
[31] Z. F. Liu, G. M. Bancroft, J. S. Tse, and H. Ågren, Phys. Rev. A **51**, 439 (1995).
[32] *Gmelin Handbook of Inorganic Chemistry, Phosphorus Suppl. Vol. C 1*, 8th ed., edited by W. Behrendt, U. W. Gerwarth, R. Hauboldt, J. v. Jouanne, H. Keller-Rudek, D. Koschel, H. Schäfer, and J. Wagner (Springer, Berlin, 1993), p. 315.
[33] J. A. Tossell and J. W. Davenport, J. Chem. Phys. **80**, 813 (1984).
[34] H. Ishikawa, K. Fujima, H. Adachi, E. Miguachi, and T. Fújii, J. Chem. Phys. **94**, 6740 (1991).
[35] P. Morin and I. Nenner, Phys. Rev. Lett. **56**, 1913 (1986).
[36] H. Aksela, S. Aksela, M. Ala-Korpela, O.-P. Sairanen, M. Hotokka, G. M. Bancroft, K. H. Tan, and J. Tulkki, Phys. Rev. A **41**, 6000 (1990).
[37] H. Aksela, S. Aksela, A. Naves de Brito, G. M. Bancroft, and K. H. Tan, Phys. Rev. A **45**, 7948 (1992).
[38] A. Naves de Brito and H. Ågren, Phys. Rev. A **45**, 7953 (1992).
[39] G. G. B. de Souza, P. Morin, and I. Nenner, Phys. Rev. A **34**, 4770 (1986).
[40] V. A. Yavna, V. A. Popov, S. A. Yavna, and L. A. Demekhina, Opt. Spektrosc. (USSR) **74**, 413 (1993).
[41] A. J. Colussi, J. R. Morton, and K. F. Preston, J. Chem. Phys. **62**, 2004 (1975).
[42] J. M. Howell and J. F. Olsen, J. Am. Chem. Soc. **98**, 7119 (1976).
[43] D. Gonbeau, M.-F. Guimon, J. Ollivier, and G. Pfister-Guillouzo, J. Am. Chem. Soc. **108**, 4760 (1986).
[44] A. Demolliens, O. Eisenstein, P. C. Hilberty, J. M. Lefour, G. Ohanessian, S. S. Shaik, and F. Volatron, J. Am. Chem. Soc. **111**, 5623 (1989).
[45] C. J. Cramer, J. Am. Chem. Soc. **113**, 2439 (1991).
[46] L. S. Bartell, J. Chem. Educ. **45**, 754 (1968).
[47] E. Hutchisson, Phys. Rev. **36**, 410 (1930).
[48] E. Hutchisson, Phys. Rev. **37**, 45 (1931).
[49] Gad Fisher, *Vibronic Coupling* (Academic, London, 1984), p. 77.
[50] E. B. Wilson, J. C. Decius, and P. C. Cross, *Molecular Vibrations* (Dover, New York, 1955).
[51] J. L. Duncan and I. M. Mills, Spectrochim. Acta **20**, 523 (1964).
[52] N. B. Colthup, L. H. Daley, and S. E. Wiberley, *Introduction to Infared and Raman Spectroscopy*, 3rd ed. (Academic, Boston, 1990).
[53] *Gmelin Handbook of Inorganic Chemistry, Silicon Suppl. Vol. B 1* (Ref. [18]), p. 98.
[54] J. R. Durig, D. J. Antion, and F. G. Baglin, J. Chem. Phys. **49**, 666 (1968).
[55] V. G. Trofimenko and V. P. Morozov, Opt. Spektrosc. (USSR) **25**, 102 (1968).
[56] *Structure Data of Free Polyatomic Molecules*, edited by K. Kuchitsu, Landolt-Börnstein, New Series, Group II, Vol. 21 (Springer, Berlin, 1992), p. 96.
[57] *Structure Data of Free Polyatomic Molecules*, edited K.-H. Hellwege and A. M. Hellwege, Landolt-Börnstein, New Series, Group II, Vol. 15 (Springer, Berlin, 1987), p. 118.
[58] *Gmelin Handbook of Inorganic Chemistry, Phosphorus Suppl. Vol. C 1* (Ref. [32]), p. 321.